

Simulating the transport and dispersal of volcanic ash clouds with initial conditions created by a 3D plume model

Zhixuan Cao^{1,2} Marcus Bursik³ Qingyuan Yang^{4,5} Abani Patra^{*,1,6}

¹ Mechanical and Aerospace Engineering Department, SUNY Buffalo, Buffalo, NY, USA

² Fluids Business Unit, ANSYS Inc, Lebanon, NH, USA

³ Center for Geohazards Studies, SUNY Buffalo, Buffalo, NY, USA

⁴ Earth Observatory of Singapore, Singapore, Singapore

⁵ The Asian School of the Environment, Nanyang Technological University, Singapore, Singapore

⁶ Data Intensive Studies Center, Tufts University, Medford, MA, USA

Correspondence*:

Abani Patra

abani.patra@tufts.edu

2 ABSTRACT

VATD (volcanic ash transport and dispersion) models simulate atmospheric transport of ash starting from a source originating at the volcano represented by concentration of ash with height. Most VATD models use a source of some prescribed shape calibrated against an empirical expression for the height-mass eruption rate (MER) relation. The actual vertical ash distribution in volcanic plumes usually varies from case to case and have complex dependencies on eruption source parameters and atmospheric conditions. We present here for the first time the use of a 3D (three-dimensional) plume model to represent the ash cloud source without any assumption regarding plume geometry. By eliminating assumed behavior associated with a semi-empirical plume geometry, the predictive skill of VATD simulations is greatly improved. To date, no VATD simulation adopts initial conditions created from first principles based on a 3D plume simulation. We use our recently developed volcanic plume model based on a 3D smoothed-particle hydrodynamic Lagrangian method, and couple the output to a standard Lagrangian VATD model. We apply the coupled model to historical eruptions to illustrate the effectiveness of the approach. Our investigation reveals that initial particle distribution in the vertical direction has more impact on transport of ash clouds than does the horizontal distribution. Comparison with satellite data indicates that ash particles are concentrated through the depth of the volcanic umbrella cloud, and much lower than observed maximum plume height.

Keywords: VATD, volcano, 3D plume model, initial conditions, numerical simulation, SPH, Pinatubo, ash transport, ash dispersal

1 INTRODUCTION

Volcanic ash, the fine-grained fraction of tephra can be widely dispersed to synoptic and global scales, and can lead to a degradation of air quality and pose threats to aviation (Tupper et al., 2007). Identification, tracking and modeling the future movement of volcanic ash help route and schedule flights to avoid ash

24 clouds. Numerical estimation of ash distribution using known and forecast wind fields is necessary if we
25 are to accurately predict ash cloud propagation and spread. Numerous VATD (volcanic ash transport and
26 dispersion) models have been developed by both civil and military aviation, and meteorological agencies to
27 provide forecasts of ash cloud motion (Witham et al., 2007). New techniques have been integrated into
28 VATDs to satisfy increasing demands for different types of output, model accuracy and forecast reliability.
29 This contribution explores a method for creating initial conditions for VATD simulations, which promises
30 to improve prediction capability.

31 Fero et al. (2009) and Stohl et al. (2011) showed that initial source conditions have significant effects on
32 simulation of volcanic ash transport. Traditional VATD simulation requires key global descriptors of the
33 volcanic plume, especially plume height, grain size, eruption duration and mass loading, or alternatively, a
34 mass eruption rate (MER). No matter how these global descriptors are obtained, they are used to furnish the
35 initial conditions for VATDs in the form of a line-source term of a spatio-temporal distribution of particle
36 mass. It is a common practice to pick values for these global descriptors using an empirical expression for
37 the height-MER relation. The empirical expression is written as a function of several parameters, including
38 the key global descriptors. The values for the descriptors can also be found by parameter calibration (e.g.
39 Fero et al., 2008, 2009; Stohl et al., 2011; Zidikheri et al., 2017). One-dimensional (1D) plume models
40 serve as an alternative option to provide values. For example, Bursik et al. (2012) used the 1D model puffin
41 (Bursik, 2001) to generate estimates of mass eruption rate and grain size. In some cases, an extra step is
42 adopted to spread ash particles from the line source horizontally, resulting in an initial ash cloud in 3D
43 space. The horizontal spreading depends on an empirical expression. For example, the VATD model Puff
44 spreads particles from the line source uniformly in the horizontal direction within a given radius using
45 an empirical expression generated from the output of puffin. Considering the complexities of volcanic
46 eruptions, the actual ash distribution in the initial ash cloud should vary from case to case and with time,
47 making it difficult to find one general expression that is suitable for all cases. It is useful therefore to
48 investigate alternative ways for creating initial ash clouds without assumptions regarding plume geometry,
49 or numerical inversion. This provides the major motivation of this paper.

50 VATD models can be categorized into Lagrangian particle tracking and Eulerian advection-diffusion
51 types. Among several available particle tracking models (e.g. Walko et al., 1995; Searcy et al., 1998;
52 D'amours, 1998; Draxler and Hess, 1998) and advection-diffusion models (e.g. Bonadonna and Houghton,
53 2005; Folch et al., 2009; Schwaiger et al., 2012), we adopt a particle tracking model, Puff (Tanaka, 1991;
54 Searcy et al., 1998), as the primary VATD model. Puff can accept a 3D point cloud description of the
55 starting ash cloud as an initial condition, which makes it technically easier to couple with 3D plume models.
56 Puff initializes a discrete number of tracers that represent a sample of the eruption cloud, and calculates
57 transport, turbulent dispersion, and fallout for each representative tracer. A cylinder emanating vertically
58 from the volcano summit to a specified maximum height is the standard approach to provide a simple model
59 of the geometry of a typical ash column. Puff minimally requires horizontal wind field data. The “restart”
60 feature of Puff makes it technically feasible to accommodate the hand-off between a plume simulation and
61 the Puff simulation in terms of time and length scales.

62 We also implement one of the most widely used models for atmospheric trajectory and dispersion
63 calculations, the Hybrid Single-Particle Lagrangian Integrated Trajectory model (HYSPLIT) (Stein et al.,
64 2015; Rolph et al., 2017), developed by NOAA’s Air Resources Laboratory. HYSPLIT is able to simulate
65 phenomena from simple back trajectories, to very sophisticated computations of transport, mixing, chemical
66 transformation, and deposition of pollutants and hazardous materials. It is used in this study to better
67 understand simulation results from Puff.

68 Besides parameter calibration, 1D plume models have been used to obtain global descriptors of volcanic
69 plumes. 1D plume models (e.g. Woods, 1988; Bursik, 2001; Mastin, 2007; de'Michieli Vitturi et al., 2015;
70 Folch et al., 2016; Pouget et al., 2016) solve the equations of motion in 1D using simplifying assumptions,
71 and hence depend on estimation of certain parameters, especially those related to the entrainment of air,
72 which is evaluated based on two coefficients: a coefficient due to turbulence in the rising buoyant jet, and
73 one due to the crosswind field. Different 1D models adopt different entrainment coefficients based on a
74 specific formulation or calibration against well-documented case studies. The feedback from plume to
75 atmosphere is usually ignored in 1D models. While these 1D models generated well-matched results with
76 3D models for plumes that are dominated by wind (often called weak plumes) much greater variability
77 is observed for strong plume scenarios (Bursik et al., 2009; Costa et al., 2016). On the other hand, 3D
78 numerical models for volcanic plumes based on first principles and having few parametrized coefficients
79 (Oberhuber et al., 1998; Neri et al., 2003; Suzuki et al., 2005; Cerminara et al., 2016a; Cao et al., 2018)
80 naturally create a 3D ash cloud, which could serve directly as an initial state of the volcanic material for
81 VATDs. However, there is no VATD simulation using such 3D ash clouds as initial conditions. In this paper,
82 we will carry out VATD simulations using an initial state for the ash cloud based on 3D plume simulations,
83 generated with Plume-SPH (Cao et al., 2018, 2017). The implementation techniques described in this paper
84 can be applied to any combination of VATD model and 3D plume model even though our investigation is
85 based on a specific VATD model and plume model.

86 The 1991 eruption of Pinatubo volcano is used as a case study. Pinatubo erupted between June 12 and 16,
87 1991, after weeks of precursory activity. The climactic phase started on June 15 at 0441 UTC and ended
88 around 1341 UTC (Holasek et al., 1996a). The climactic phase generated voluminous pyroclastic flows,
89 and sent Plinian and co-ignimbrite ash and gas columns to great altitudes (Scott et al., 1996). The evolution
90 of the Pinatubo ash and SO_2 clouds was tracked using visible (Holasek et al., 1996a), ultraviolet (Total
91 Ozone Mapping Spectrometer; TOMS) (Guo et al., 2004a) and infrared sensors, including the Advanced
92 Very High-Resolution Radiometer (AVHRR) (Guo et al., 2004b). There is sufficient observational data to
93 estimate the eruption conditions for the climactic phase of the eruption (Suzuki and Koyaguchi, 2009). The
94 availability of calibrated eruption conditions and extensive observational data regarding ash cloud transport
95 make the Pinatubo eruption an ideal case study.

2 MATERIALS AND METHODS

96 2.1 Plume-SPH Model

97 Plume-SPH (Cao et al., 2018) is designed to describe an injection of well mixed solid and volcanic gas
98 from a circular vent above a flat surface into a stratified stationary atmosphere. The basic assumptions of
99 the model are:

- 100 1. Molecular viscosity and heat conduction is neglected since turbulent energy and momentum exchange
101 are dominant.
- 102 2. Erupted material consisting of solid with different size and mixture of gases is assumed to be well
103 mixed and behave like a single phase fluid (phase 2) which is valid for eruptions with fine particles and
104 ash.
- 105 3. Air, which is assumed to be well mixed mixture of different gases, is assumed to be another phase
106 (phase 1).
- 107 4. Assume thermodynamic equilibrium and dynamic equilibrium between the two phases. As a result,
108 both phases share the common energy equation and momentum equations.

- 109 5. All other microphysical processes (such as the phase changes of H₂O aggregation, disaggregation,
 110 absorption of gas on the surface of solids, solution of gas into a liquid) and chemical processes are not
 111 considered in this model.
 112 6. The effect of wind, is also not yet considered in this model.

Based on above assumptions, the governing equations of our model are given as:

$$\frac{\partial \rho}{\partial t} + \nabla \cdot (\rho \mathbf{v}) = 0 \quad (1)$$

$$\frac{\partial \rho \xi}{\partial t} + \nabla \cdot (\rho \xi \mathbf{v}) = 0 \quad (2)$$

$$\frac{\partial \rho \mathbf{v}}{\partial t} + \nabla \cdot (\rho \mathbf{v} \mathbf{v} + p \mathbf{I}) = \rho \mathbf{g} \quad (3)$$

$$\frac{\partial \rho E}{\partial t} + \nabla \cdot [(\rho E + p) \mathbf{v}] = \rho \mathbf{g} \cdot \mathbf{v} \quad (4)$$

113 where ρ is the density, \mathbf{v} is the velocity, ξ is the mass fraction of ejected material, \mathbf{g} is the gravitational
 114 acceleration, \mathbf{I} is a unit tensor. $E = e + K$ is the total energy which is a summation of kinetic energy K
 115 and internal energy e . An additional equation is required to close the system. In this model, the equation
 116 for closing the system is the following EOS (equation of state).

$$p = (\gamma_m - 1) \rho e \quad (5)$$

117 where

$$\gamma_m = R_m / C_{vm} + 1 \quad (6)$$

$$R_m = \xi_g R_g + \xi_a R_a \quad (7)$$

$$C_{vm} = \xi_s C_{vs} + \xi_g C_{vg} + \xi_a C_{va} \quad (8)$$

$$\xi_a = 1 - \xi \quad (9)$$

$$\xi_g = \xi \cdot \xi_{g0} \quad (10)$$

$$\xi_s = \xi - \xi_g \quad (11)$$

123 where, C_v is the specific heat with constant volume, R is the gas constant. ξ is the mass fraction of erupted
 124 material. The subscript m represents mixture of ejected material and air, s represents solid portion in the
 125 ejected material, g represents gas portion in the ejected material, a represents air, 0 represents physical
 126 properties of erupted material. ξ_{g0} is the mass fraction of vapor in the erupted material.

127 Three different boundary conditions are applied in this model. At the vent, temperature of erupted
 128 material T , eruption velocity \mathbf{v} , the mass fraction of vapor in erupted material ξ_{g0} and mass discharge
 129 rate \dot{M} are given. The pressure of erupted material p is assumed to be the same as ambient pressure for
 130 pressure-balanced eruption. The radius of vent is determined from ρ , \dot{M} and \mathbf{v} . Non-slip wall boundary
 131 condition is applied to the flat ground, where we enforce the velocity to be zero. With further assumption
 132 that the ground is adiabatic, internal energy flux, which consists of heat flux and energy flux carried by
 133 mass flux, vanishes on the wall boundary. Pressure outlet boundary condition is applied to the surrounding
 134 atmosphere where the pressure is given. Except for the pressure, boundary values for density, velocity, and

135 energy are determined by numerical calculation naturally. The initial condition for Plume-SPH is created
 136 based on atmosphere profile before the eruption.

137 The governing equations, EOS, boundary conditions, and initial conditions establish a complete mathe-
 138 matic model. The model is then discretized using smoothed particle hydrodynamics (SPH) method. The
 139 discretized model is then converted into computational software (Plume-SPH) based on a parallel data
 140 management framework (Cao et al., 2017).

141 The input parameters for Plume-SPH include the eruption condition at vent, the material properties, and
 142 atmosphere profile. The eruption parameters, material properties and atmosphere for the “Strong plume–no
 143 wind” case in the recent comparison study on eruptive column models (Costa et al., 2016) are adopted.
 144 Eruption conditions and material properties are listed in Table 3. Note that the density of erupted material
 145 at the vent and radius of the vent can be computed from the given parameters. The eruption pressure is
 146 assumed to be the same as the atmospheric pressure at the vent, hence is not given in the table. The vertical
 147 profiles of atmospheric properties were based on the reanalysis data from ECMWF (European Centre for
 148 Medium-Range Weather Forecasts) for the period corresponding to the climactic phase of the Pinatubo
 149 eruption.

150 2.2 Puff and Initial Ash Cloud

151 Puff (Tanaka, 1991; Searcy et al., 1998) is a dynamic pollutant tracer model. the model is based on a 3D
 152 Lagrangian form of the fluid mechanics, in which the material transport is represented by the fluid motion,
 153 and diffusion is parameterized by a stochastic process of random walk. Here, the model is constructed by a
 154 sufficiently large number of Lagrangian tracer particles with a random variables $\mathbf{R}_i(t) = (x(t), y(t), z(t))$,
 155 where $i = 1 \sim M$, which represent position vectors of particles from the origin of the ash source at the
 156 time t . M is total number of Lagrangian tracer particles, a sample of all the ash particles.

$$157 \quad \mathbf{R}_i(t + \Delta t) = \mathbf{R}_i(t) + \mathbf{W}(t)\Delta t + \mathbf{Z}(t)\Delta t + \mathbf{S}_i(t)\Delta t \quad (12)$$

158 Here, \mathbf{W} accounts for wind advection, \mathbf{Z} is generated by Gaussian random numbers and accounts for
 159 turbulent dispersion, and \mathbf{S} is the terminal gravitational fallout velocity or settling speed, which depends on
 160 a tracer’s size.

161 To start a Puff simulation, it requires a collection of tracer particles as the initial condition, which can
 162 be generated by Puff according to several parameters given by user. The tracer particles has three basic
 163 properties, age, size and position. The age of each particle is the elapsed time from when they were released
 164 from the site. Ash particles in the initial ash cloud has zero ages. Ash size distribution is initialized using a
 165 Gaussian shape on a logarithmic scale. According to mean and standard deviation provided by user, Puff
 166 will assign size to each particle. Puff initialize the position of each particle according to semiempirical
 167 expressions. The height of each particle is determined according to specified distribution from the surface
 168 ($1000\text{mbar} \cong 0\text{m}$) to the top of the plume height, H_{max} , which is given by user.

169 The most commonly used distribution in Puff is Poisson distribution. For the Poisson distribution, the
 170 vertical height of ash particles is given by Eq. (13):

$$171 \quad H = H_{max} - 0.5H_{width} * P + H_{width}R \quad (13)$$

172 where P is an integral value drawn from a Poisson distribution of unit mean, R is a uniformly distributed
 173 random number between 0 and 1, H_{max} is the maximum plume height, H_{width} represents an approximate
 vertical range over which the ash will be distributed. Another commonly used vertical ash distribution

174 in VATD simulation is Suzuki. For the Suzuki plume shape (Suzuki et al., 1983), the ash mass vertical
 175 distribution is assumed to follow the Eq. (Eq. (14)):

$$Q(z) = Q_m * \frac{k^2(1 - z/H_{max})\exp(k(z/H_{max} - 1))}{H_{max}[1 - (1 + k)\exp(-k)]} \quad (14)$$

176 Where Q_m is the total mass of erupted material, k is shape factor, which is an adjustable constant that
 177 controls ash distribution with height. A low value of k gives a roughly uniform distribution of mass with
 178 elevation, while high values of k concentrate mass near the plume top. For Poisson distribution, besides
 179 the plume height H_{max} , there is another user specified parameter, H_{width} , which also affect the vertical
 180 ash distribution. For Suzuki distribution, besides the plume height H_{max} , there is another user specified
 181 parameter, k , which also affect the vertical ash distribution.

182 Puff initialize the horizontal distribution of ash particles according to semiempirical expression as well.
 183 Puff uses a uniformly distributed random process to determine ash particle locations in a circle centered
 184 on the volcano site. The maximum radius (at plume top) at which a particle can be located is given as
 185 “horizontal spread”. The horizontal displacement from a vertical line above the volcano is a random value
 186 within a circle of which the radius equals the “horizontal spread” multiplied by the ratio of the particle
 187 height H to the maximum H_{max} . So the resulting shape of the particle distribution within the plume is an
 188 inverted cone in which particles are located directly over the volcano at the lowest level and extend out
 189 further horizontally with increasing plume height.

$$r(H) = r_{max} * H/H_{max} * R \quad (15)$$

190 where $r(H)$ is the radius of the horizontal circle, whthin which, all particles at the height of H locate.
 191 r_{max} is the horizontal spread. H is the height, R is an uniformly distributed random number between 0 and
 192 1.

193 In summary, given user has chosen Posisson distribution for particle distribution in the vertical direction,
 194 there are three user specified parameters that control the tracer particle distribution in the initial ash cloud:
 195 H_{max} , H_{width} , and r_{max} . User can optimize or calibrate these parameters to adjust the initial condition of
 196 Puff so that the simulated results match better with observations, such as satellite imagery or pilot reports.
 197 Except for the initial ash cloud, there are several other parameters that control Puff simulation process.
 198 These parameters are list in Table 4.

199 2.3 Creation of Initial Ash Cloud

200 The steps to create an initial ash cloud based on the raw output of Plume-SPH are shown in Fig. 1.
 201 The method proposed consists in generating the initial ash cloud directly from Plume-SPH, foregoing
 202 assumptions and estimates, or inverse modeling, regarding ash injection height and timing. We use Plume-
 203 SPH as an example, noting that for other 3D plume models, the steps would be similar. Plume-SPH is a
 204 two-phase model based on the Lagrangian smoothed-particle hydrodynamics (SPH) method, in which the
 205 computational domain is discretized by SPH particles. The current version, Plume-SPH 1.0 (Cao et al.,
 206 2018), uses two types of SPH particles: 1) particles of phase 1 to represent ambient air, and 2) particles of
 207 phase 2 to represent erupted material. The initial ash cloud is created from SPH particles of phase 2.

208 After reaching the maximum rise height and starting to spread horizontally, particles of phase 2 form an
 209 initial umbrella cloud (Fig. 2). The 3D plume simulation is considered complete once the umbrella cloud
 210 begins to form. Parcels that will be transported by the ambient wind are those above the “corner” region,
 211 where mean plume motion is horizontal rather than vertical.

212 Considering that SPH particles are only discretization points, each is assigned a grain size according to a
213 given total grain size distribution (TGSD) (Paladio-Melosantos et al., 1996), and a concentration according
214 to the mass and volumetric eruption rate. The Plume-SPH discretization points are thus switched to Puff
215 Lagrangian tracer particles having grain sizes and concentrations. The coordinates of these tracer particles,
216 which are initially in the local Cartesian coordinate system of Plume-SPH, are converted into Puff's global
217 coordinate system, which is given in terms of (*longitude, latitude, height*). Puff takes the initial ash
218 cloud, consisting of the collection of Lagrangian tracer particles with grain size and concentration, and
219 propagates from time t to time $t + \Delta t$ via solution to an advection/diffusion equation.

220 To summarize, there are four steps to create an initial ash cloud from the raw output of Plume-SPH:

- 221 1. filter by SPH particle type to select SPH particles that represent erupted material (phase 2)
- 222 2. filter by a mean velocity threshold to select the upper part (above the “corner” region) dominated by
223 horizontal transport
- 224 3. switch SPH discretization points to Lagrangian tracer particles, by assigning grain size to each particle
- 225 4. convert coordinates of the SPH Lagrangian tracers into the VATDs' geographic coordinate system

226 The features of the volcanic plume and resulting initial ash cloud used in the case study are shown in Fig. 2.
227 It is important to point out that since both Plume-SPH and Puff are based on the Lagrangian method, there
228 is no extra step of conversion between an Eulerian grid and Lagrangian particles.

229 Table 1 compares three different methods for creating initial conditions for a VATD simulation: 1) 230 creating initial conditions based on parameter calibration without any plume model (method 1), 2) creating
231 initial conditions based on output of a 1D plume model (method 2), 3) extracting an initial ash cloud from
232 a 3D plume simulation (method 3). The first method determines all global descriptors of volcanic plumes
233 based on calibration. An initial line source or ash cloud is then created according to a semiempirical plume
234 shape expression. Both of the other two methods depend on plume models. However, 3D plume models
235 can generate initial ash clouds in 3D space, while 1D plume models only generate global descriptors of
236 a plume, so a semiempirical expression or transformation is still needed to create a 3D initial ash cloud.
237 In addition, the number of Lagrangian tracers is a free parameter when using semiempirical plume shape
238 expressions, while it depends on a computationally optimized simulation when generating them from the
239 output of a 3D plume simulation.

240 2.4 Puff Restart

241 The plume and ash transport models are run at different time scales and length scales. The spatial and
242 temporal resolutions of the plume simulations are much finer than those of the ash transport model. It takes
243 tens of minutes (600s in this case) for the Pinatubo plume to reach a steady height. However the eruption
244 persisted for a few hours (9 hours for the climactic phase of Pinatubo eruption), and it may be necessary
245 to track ash transport for days following an eruption. At present, it is too expensive computationally to
246 do 3D plume simulations of several hours in real time. In order to handle the difference in time scale, we
247 mimic a continuing eruption with intermittent pulses releasing ash particles. In particular, we restart Puff at
248 an interval of 600s, i.e., the physical time of the plume simulation to reach a steady height. At every Puff
249 restart, we integrate the output of the last Puff simulation and Plume-SPH into a new ash cloud. This new
250 ash cloud serves as a new initial condition with which to restart a Puff simulation. A sketch demonstrating
251 the overall restart process is shown in Fig. (3). The total number of Lagrangian tracer particles used in Puff
252 thus equals the summed number of particles in all releases. The total number of tracer particles is therefore
253 no longer a user-selected parameter. Fero et al. (2008) proposed using more realistic time-dependent plume

254 heights. We do not adopt that strategy here for simplicity, although the idea would be straightforward in
255 execution, given time-dependent eruption conditions.

3 RESULTS

256 Transport of volcanic ash resulting from the Pinatubo eruption on June 15, 1991, is simulated using two
257 different initial conditions. The first type of initial condition is created in a traditional way according to
258 key global descriptors (H_{max} , H_{width} and r_{max}) and the semiempirical plume shape expressions. We use
259 the observed top height (40km) and two other parameters assigned semiempirically (Bursik et al., 2012).
260 The second type of initial condition is created by the new method proposed in this paper. To create initial
261 conditions using the new method described in this paper, the plume rise is simulated first by Plume-SPH.
262 Then the initial ash cloud is obtained by processing the raw output of Plume-SPH following steps described
263 in Sec. 2.3. Except for initial conditions, the simulation parameters that control the VATD simulation are
264 the same for both simulations. Simulated ash transport results are compared against observations.

265 The simulation results using different initial conditions are compared with TOMS images and AVHRR
266 BTD ash cloud map imagery (Fig. 6). The differences between simulated ash transport by the “Semiempirical
267 initial cloud + Puff” and “Plume-SPH+ Puff” conditions are significant. The simulated ash concentration
268 based on the initial conditions created from Plume-SPH is qualitatively closer to observation than that
269 based on the semiempirical plume shape expression. At 23 hours and 31 hours after the beginning of the
270 climactic phase, the “Plume-SPH + Puff” simulation generates ash footprints that are closer to observations,
271 especially in forecasting the location where there is a high concentration of ash. However, ash just west of
272 Pinatubo observed in satellite images does not show up in “Plume-SPH + Puff” simulation results. This
273 disparity is likely due to the fact that Pinatubo continued erupting after the climactic phase, while we only
274 simulate the climactic phase. The “Semiempirical initial cloud + Puff” simulation, however, forecasts an
275 ash distribution more spatially restricted than observation. The location of the high concentration region
276 is far northwest of observation. Around 55 hours after the beginning of the climactic phase, the disparity
277 between observation and simulation becomes more obvious. Ash in the “Semiempirical initial cloud + Puff”
278 simulation is located too far west of the observation. The high concentration area of the “Plume-SPH +
279 Puff” simulation, even though closer to observation than that of the “Semiempirical initial cloud + Puff”
280 simulation, has also propagated further than observation.

281 Except for the initial conditions, both simulations adopt the same parameters and wind field data. That is
282 to say, the only difference between these two simulations is the initial distribution of ash parcels. The main
283 difference between simulation results from the “Plume-SPH + Puff” and the “Semiempirical initial cloud +
284 Puff” runs can be directly attributed to the initial ash particle distribution, which we discuss in detail in the
285 following section.

4 DISCUSSION

286 4.1 Importance of Maximum Height (H_{max})

287 In this section, we discuss the vertical distribution of ash particles in the initial ash cloud. The majority of
288 volcanic ash particles are usually injected at an elevation lower than the maximum height. For instance,
289 Holasek et al. (1996a,b) reported the maximum Pinatubo plume height as $\sim 39\text{km}$ while the cloud heights
290 were estimated at $\sim 20 - 25\text{ km}$. Self et al. (1996) reported that the maximum plume height could have
291 been $> 35\text{ km}$, but that plume heights were $23 \sim 28\text{ km}$ after $\sim 15 - 16\text{ hours}$. The neutral buoyancy
292 height of the Pinatubo aerosol cloud was estimated with different methods at: $\sim 17 - 26\text{km}$ (lidar) by
293 DeFoor et al. (1992), $\sim 20 - 23\text{ km}$ (balloon) by Deshler et al. (1992), $\sim 17 - 28\text{ km}$ (lidar) by Jäger

294 (1992), and $\sim 17 - 25\text{km}$ (lidar) by Avdyushin et al. (1993). Based on comparison between simulated
295 clouds with early infrared satellite imagery of Pinatubo, Fero et al. (2008) reported that the majority of ash
296 was transported between 16 km and 18 km. These observations make good physical sense, as particles are
297 concentrated near the intrusion height of the umbrella cloud, not near the plume top, because the plume top
298 is due to momentum overshoot. However, the empirical expressions for the height-MER relation, which
299 are commonly adopted to create initial conditions for VATD simulations, tend to place the majority of ash
300 particles closer to the top if one uses observed maximum height in the empirical expressions.

301 Here we investigate two commonly used plume shapes, the Poisson and Suzuki. Particle distributions
302 (in terms of mass percentage or particle number percentage) in the vertical direction in the initial ash
303 cloud are shown in Fig. 7. In that figure, the vertical particle distribution based on Plume-SPH output is
304 compared with the vertical particle distribution created based on semiempirical shape expressions. Both
305 Poisson and Suzuki distributions in Fig. 7 take $H_{max} = 40\text{ km}$, which is close to the reported observation
306 of maximum height. When adopting the Poisson distribution, see (c) in Fig. 7, the majority of the particles
307 are between $30\text{km} \sim 40\text{km}$. Obviously, the Poisson function distributes the majority of ash at a higher
308 elevation than was observed (e.g. Fero et al., 2008). As for the Suzuki distribution, (d) in Fig. 7, the
309 majority of ash particles also occur in a range that is significantly higher than 25 km. As for initial ash
310 clouds based on Plume-SPH simulation, most ash particles are distributed between $\sim 17 - 28\text{ km}$, which
311 matches well with observations. The maximum height is also consistent with observation. To summarize,
312 using a semiempirical plume shape expression generates an unrealistic initial ash cloud even if we use the
313 observed maximum plume height.

314 For the Poisson and Suzuki distributions, the maximum in ash particles cannot be lower without changing
315 the maximum height. To distribute the majority of ash particles at a lower elevation, the maximum height
316 must be reduced to a value smaller than the observed maximum height. Adjusting parameters such as
317 maximum height in the empirical expression is actually the traditional source term calibration method. A
318 set of initial ash clouds using different maximum heights based on the Poisson distribution is shown in Fig.
319 8). The maximum heights adopted in plume shape expressions are not obtained from any plume model or
320 observation of plume height, but by *a posteriori* calibration to later-observed ash cloud transport heights.

321 The ash clouds created by the Poisson distribution with different maximum heights are used as initial
322 conditions in Puff simulations, whose results are shown in Fig. 11. Except for the maximum height, all
323 other parameters for creating an initial ash cloud are the same as those in Table 4. Of course, the range
324 over which the majority of ash particles is located is lower when using lower maximum heights. Figure
325 11 thus shows that the maximum height has a significant influence on the ash transport simulation. When
326 the maximum height is 10 km, the high concentration area lags behind that observed. If the designated
327 maximum height is 35 km, the high concentration area propagates faster and is more spatially confined than
328 observed. When using a maximum height of $\sim 41000\text{ m}$, the high concentration area propagates faster and
329 the footprint is narrower than in both observation and “Plume-SPH + Puff” simulation results (see Fig. 6).
330 The simulated high concentration area is closest to “Plume-SPH + Puff” simulation results when assigning
331 a maximum height of 30 km. The low-concentration front of the volcanic ash cloud propagates faster than
332 observed, and is located far west of the high concentration areas. A low concentration tail area also appears
333 in the simulation results while there is no such tail in the observed imagery, although this could be the
334 result of imagery calibration or sensitivity. Simulation results based on a calibrated maximum height of 30
335 km show a footprint similar to those of “Plume-SPH + Puff”, although smaller in terms of area. However,
336 the initial ash cloud created by a Poisson distribution with maximum height around 20 km generates the
337 best match ash with observation. That is to say, a maximum height lower than the real maximum height

is required by the Poisson plume shape to distribute ash particles at elevations comparable to the “true” ash distribution. Our hypothesis regarding the disparity between the “Semiempirical initial cloud + Puff” simulations and observation is confirmed. Since the initial condition of vertical ash distribution has such a dominant effect on VATD simulation, it is critical for the forecast capability of VATD simulations to explore more accurate and adaptive ways for establishing the initial ash distribution, especially methods that do not rely on *a posteriori* parameter calibration or inversion.

4.2 Effect of Vertical Spread (H_{width})

In the previous section, we explored the effects of adjusting the maximum height to change the vertical ash distribution at the source. In this section, we investigate the importance of another parameter in the semiempirical Poisson expression. We vary the “vertical spread” (H_{width} in Puff) in the range $\sim 3 - 10$ km. A set of initial ash clouds with different vertical spreads are shown in Fig. 8. Except for vertical spread, all other parameters for creating an initial ash cloud are the same as those in Table 4. The vertical width of the region within which the majority of ash particles are located becomes narrower when a smaller value for the vertical spread parameter is used, but changing it has no obvious effect on the height at which the largest fraction of ash particles is injected (essentially the height of a mode in ash distribution). The ash clouds based on different vertical spread parameters are then used as initial conditions in Puff simulations.

The results are shown in Fig. 11. Adjusting of the vertical spread changes particle distribution in the vertical direction, and thus, not surprisingly affects the VATD simulation results. None of the VATD simulations based on initial ash clouds with vertical spreads equal to 3, 5 or 10 km yield better results than do VATD simulations based on initial conditions created by Plume-SPH (see Fig. 11).

The calibration tests on vertical spread, carried out here, are certainly not exhaustive. One could do a more comprehensive calibration throughout the multi-dimensional parameter space (for Poisson distribution, the parameter space is two dimensional) and find better results. In addition, with a more complicated semiempirical plume shape expression, one could have more control over plume shape and might be able to get an initial condition that yields a more accurate ash transport forecast. However, more complicated and adaptable plume shape expressions imply a higher dimensional parameter space, which requires more effort in calibration, even though the degrees of freedom to adjust plume shape are still limited. Creating initial conditions based on 3D plume simulations is more adaptive to various cases and yields results as good as or better than calibration of the poorly-constrained semi-empirical parameter, vertical spread.

4.3 Horizontal Ash Distribution

The differences between the semiempirical plume particle distribution and actual (or simulated by the 3D plume model) are not only in the vertical direction. The importance of the horizontal distance of each initial ash particle from a line extending upward from the volcano is investigated in this section. Puff uses a uniformly distributed random process to determine ash particle locations in a circle centered on the volcano site as described in section 2.2. For the output of Plume-SPH, an effective (maximum) radius is determined according to a given threshold of ash concentration, following Cerminara et al. (2016b). A time averaged, spatial integration of the dynamic 3D flow field is conducted to remove significant fluctuations in time and space. Fig. 9 compares radius of the initial ash clouds created by 3D plume simulations with that assumed in the semiempirical plume shape expression adopted in Puff. It is impossible for the simple, assumed plume shapes to capture the complex and more realistic shapes developed by Plume-SPH. Additional parameterization may generate more reasonable shapes, but these would continue to be *ad hoc*, none would likely to have the potential fidelity of the 3D simulation to reality, and adding a temporally changing distribution would be difficult.

381 Comparison between cross-sectional views of the initial ash clouds is shown in Fig. 10. The cross-
382 sectional view of horizontal particle distribution using the semiempirical method (last figure in Fig. 10)
383 is similar to a cross-sectional view of a simulated 3D plume, in a general sense. However, for simulated
384 3D plumes, the ash particle distribution in cross section varies with height, which factor would become
385 increasingly important with increasing wind speed, were wind speed to be included in the estimate of initial
386 plume shape. It is difficult for the semiempirical expressions to accommodate such a complex distribution.

387 Despite the obvious difficulty of correctly estimating ash distribution near the vent, or for short propagation
388 times, assigning different values for the horizontal spread has a negligible effect on VATD simulation
389 results at large time. We investigated horizontal spread values between 50 km and 1600 km to create initial
390 ash clouds; all of them generated similar results at large propagation times (> 1 day). Figure 11 shows two
391 different simulation results based on initial ash clouds with horizontal spread equal to 50 km and 600 km,
392 respectively. No visible differences are apparent between them. This implies that horizontal distribution
393 has a less significant influence on VATD simulation results than does vertical distribution for long distance
394 or large time. Perhaps the most important ramification of this result is that it means the time at which the
395 “handshake” is made between Plume-SPH and the VATD does not affect results significantly for relatively
396 large distances and times.

397 4.4 Sensitivity Analysis of Other Parameters

398 Besides the positions of particles in the initial ash cloud, other parameters for Puff simulations are:
399 horizontal diffusivity, vertical diffusivity, mean grain size, grain size standard deviation and total number
400 of tracers. We present in this subsection informal but systematic sensitivity studies on these parameters.
401 We also investigate the influence of eruption duration. The sensitivity analyses will serve as the basis for
402 identifying possible sources of disparities between simulation and observation.

403 The sensitivity analyses illustrate that adjustment of parameters other than the positions of particles in
404 the initial ash cloud produces negligible visual differences in VATD simulation results. Using horizontal
405 diffusivities in the range of $[100, 100000] m^2 s^{-1}$ and vertical diffusivities in the range of $[1, 20] m^2 s^{-1}$
406 produces visually negligible differences. The simulated eruption duration should depend on either the total
407 observed duration or the duration of the climactic phase. We conducted several simulations with eruption
408 duration varying in the range of [5, 11] hours with slightly different starting time of climactic phase. Table
409 2 lists all these simulations. However, only slight visible differences are observed among the simulated ash
410 transport outputs. The mean of the grain size distribution also has visually negligible effects on long-term
411 ash transport, according to our sensitivity tests in which we varied the log mean (base 10) grain radius in
412 the range of $[-7.3, -3.5] m$. The standard deviation, when varying in the range of $[0.1, 10] m$, generates a
413 negligible difference on long-range ash transport as well. A similar conclusion on parameter sensitivity is
414 reported by Fero et al. (e.g. 2008); Daniele et al. (e.g. 2009). Among the parameters explored, the eruption
415 duration and beginning time show the most obvious influence on simulated ash distribution, although the
416 effect is still small. To show the differences in an intuitive way, (a) - (c) in Fig. ?? shows simulated ash
417 distribution corresponding to 4.9 hours duration, 9 hours duration and 11 hours duration, respectively.
418 After 72 hours, relative to the simulation starting time, these three cases generate very similar results
419 with tiny visible differences. To summarize, all these parameters have negligible effects on long-term ash
420 distribution.

421 The new methodology for generating initial ash clouds introduces a new parameter: elevation threshold,
422 which is the lower elevation limit of the ash that will be transported by the VATD. This parameter needs to be
423 specified at this time, as there is no *a priori* way to define it, given the continuous vertical distribution of ash
424 in the eruption column. We carry out a separate, informal sensitivity analysis on this parameter by varying

425 the elevation threshold from 1500 m (the height of the vent) to 25000 m. The simulated ash distributions
426 show obvious visible differences. Such influence is especially obvious when the elevation threshold is
427 either very high or very low. However, varying the elevation threshold in the range of [12000, 18000] m
428 generates relatively small differences in ash transport simulation results. Figure 4 (d) and (e) compare the
429 simulated ash distributions corresponding to elevation thresholds of 1500 m and 15000 m. Compared with
430 the ash distribution for a threshold of 25000 m, an extra long tail appears when using an elevation threshold
431 of 1500 m. Adopting lower elevation thresholds adds more tracer particles at lower elevation. As the winds
432 at different elevations are different, the tracers at lower elevations propagate in different directions. The
433 HYSPLIT (Stein et al., 2015; Rolph et al., 2017) forward trajectory tracking starting at 1624 UTC on
434 June 15, indicates that the wind between elevations of 10000 m and 15000 m blew from north-east to
435 south-west, while winds of higher elevation blew from east to west (see Fig. 5). The results suggest that the
436 elevation threshold is best estimated from the height at which the parcel number or mass concentration has
437 an inflection point in the vertical distribution (*cf.* Figure 4(d) and (e)). Below this inflection point, particle
438 trajectories are primarily vertical in the stalk-like eruption column. Above this level, particle trajectories
439 are primarily horizontal, as they flow into the umbrella cloud gravity current.

440 The sensitivity analyses demonstrate that the initial conditions for the VATD simulations, derived from
441 the plume model, have the most significant effect on simulated ash propagation, while all other input
442 parameters have negligible influence. An initial ash cloud generated based on the semiempirical expression,
443 which is a function of several parameters, often differs significantly from a realistic initial ash cloud. Such
444 initial conditions might greatly compromise the accuracy of a VATD simulation.

445 In this paper, we do not carry out any sensitivity investigation with respect to wind field, even though it is
446 a dominant factor in a VATD simulation. In the present case study, we use global NOAA/OAR/ESRL6–
447 h , 2.0° reanalysis wind field data (Whitaker et al., 2004; Compo et al., 2006, 2011).

448 4.5 Summary

449 This paper presents, for the first time, VATD simulations using initial source conditions created by a 3D
450 plume model. Traditional VATD simulations use initial conditions created according to a semiempirical
451 plume shape expression. A case study of the 1991 Pinatubo eruption demonstrates that a 3D plume model
452 can create more realistic initial ash cloud and ash parcel positions, and therefore improve the accuracy of
453 ash transport forecasts. Informal sensitivity analyses suggest that initial conditions, as expressed in the
454 disposition of initial ash parcel positions in the vertical, have a more significant effect on a volcanic ash
455 transport forecast than most other parameters. Comparison of initial ash parcel distributions among the
456 3D plume model, semiempirical expressions, and observations suggests that a major subpopulation of ash
457 parcels should be placed at a much lower elevation than maximum height to obtain a better VATD forecast.
458 For the Pinatubo case study, “well-matched” simulation results are observed when using a maximum height
459 of around 30 km in semiempirical expressions, which is much lower than the observed maximum height of
460 40 km. Comparing the effects of the maximum height, vertical spread and horizontal spread shows that ash
461 particle distribution in the vertical direction has the strongest effect on VATD simulation.

462 To summarize, we have presented a novel method for creating *a priori* initial source conditions for
463 VATD simulations. We have shown that it might be possible to obtain initial positions of ash parcels
464 with deterministic forward modeling of the volcanic plume, potentially obviating or lessening the need to
465 attempt to somehow observe initial positions, or *a posteriori* create a history of release heights via inversion
466 (Stohl et al., 2011). Although the method now suffers from the high computational cost associated with
467 3D forward modeling, there is the possibility that in future it might not only help overcome shortcomings
468 of existing methods used to generate *a priori* input parameters, but also overcome the need to do the

469 thousands of runs associated with inverse modeling. In addition, computational cost will continue to
470 diminish as computing speed increases. As they are forward numerical models based on first principles,
471 3D plume models need little if any parameterization, and user intervention should not be required to
472 improve forecast power; no assumption about the initial position of ash parcels is needed. Generation of the
473 initial cloud of ash parcels directly by 3D simulation is potentially adaptable to a variety of volcanic and
474 atmospheric scenarios. In contrast, semiempirical expressions used to determine initial conditions require
475 several parameters to control ash particle distribution along a vertical line source or some simplified shape
476 of the initial ash cloud, making it difficult in some cases to generate initial conditions that closely resemble
477 a complex reality.

478 The full range of research issues raised by numerical forecasting of volcanic clouds is diverse. We
479 described in this paper the effect of initial conditions chosen from the output of a 3D plume model on
480 numerical forecasts of volcanic ash transport simulations. The wind field, another important factor in
481 volcanic ash transport simulations, is not discussed in the present work. Some other aspects, such as
482 microphysical processes, even though they play lesser roles, likely need to be included in VATDs to
483 improve accuracy for a particular eruption. In addition, eruption conditions are subject to change with time,
484 even during the climactic phase of an eruption. In the future, time-dependent initial conditions for VATDs
485 can be created from 3D plume simulations with time-dependent eruption conditions.

CONFLICT OF INTEREST STATEMENT

486 The authors declare that the research was conducted in the absence of any commercial or financial
487 relationships that could be construed as a potential conflict of interest.

AUTHOR CONTRIBUTIONS

488 The idea of using 3D plume model to start a VATD simulation originated from a conservation between AP
489 and MB. ZC carried out the Plume-SPH simulations, PUFF simulations, results analysis, and prepared the
490 first draft. All authors worked together for further revisions. MB carried out the HYSPLIT simulation. QY
491 post processed the PUFF simulation results, overlapped the simulation results with satellite observation.
492 All authors contributed equally to the manuscript writing. AP and MB obtained funding to financially
493 support the work.

FUNDING

494 This work was supported by National Science Foundation awards 1521855, 1621853, and 1821311,
495 1821338 and 2004302 and by the National Research Foundation Singapore and the Singapore Ministry
496 of Education under the Research Centres of Excellence initiative (project number: NRF2018NRF-
497 NSFC003ES-010).

ACKNOWLEDGMENTS

498 Support for the Twentieth Century Reanalysis Project dataset is provided by the U.S. Department of Energy,
499 Office of Science Innovative and Novel Computational Impact on Theory and Experiment (DOE INCITE)
500 program, and Office of Biological and Environmental Research (BER), and by the National Oceanic and
501 Atmospheric Administration Climate Program Office. We are grateful to the two anonymous reviewers of
502 the paper for their constructive comments and suggestions that improved the paper.

REFERENCES

- 503 Avdyushin, S., Tulinov, G., Ivanov, M., Kuzmenko, B., Mezhuev, I., Nardi, B., et al. (1993). 1. spatial and
504 temporal evolution of the optical thickness of the pinatubo aerosol cloud in the northern hemisphere
505 from a network of ship-borne and stationary lidars. *Geophysical research letters* 20, 1963–1966
- 506 Bonadonna, C. and Houghton, B. (2005). Total grain-size distribution and volume of tephra-fall deposits.
507 *Bulletin of Volcanology* 67, 441–456
- 508 Bursik, M. (2001). Effect of wind on the rise height of volcanic plumes. *Geophys. Res. Lett* 28, 3621–3624
- 509 Bursik, M., Jones, M., Carn, S., Dean, K., Patra, A., Pavolonis, M., et al. (2012). Estimation and
510 propagation of volcanic source parameter uncertainty in an ash transport and dispersal model: application
511 to the eyjafjallajokull plume of 14–16 april 2010. *Bulletin of volcanology* 74, 2321–2338
- 512 Bursik, M., Kobs, S., Burns, A., Braitseva, O., Bazanova, L., Melekestsev, I., et al. (2009). Volcanic
513 plumes and wind: Jetstream interaction examples and implications for air traffic. *Journal of Volcanology*
514 and *Geothermal Research* 186, 60–67
- 515 Cao, Z., Patra, A., Bursik, M., Pitman, E. B., and Jones, M. (2018). Plume-sph 1.0: a three-dimensional,
516 dusty-gas volcanic plume model based on smoothed particle hydrodynamics. *Geoscientific Model
517 Development* 11, 2691–2715
- 518 Cao, Z., Patra, A., and Jones, M. (2017). Data management and volcano plume simulation with parallel
519 sph method and dynamic halo domains. *Procedia Computer Science* 108, 786–795
- 520 Cerminara, M., Esposti Ongaro, T., and Berselli, L. (2016a). Ashee-1.0: a compressible, equilibrium-
521 eulerian model for volcanic ash plumes. *Geoscientific Model Development* 9, 697–730
- 522 Cerminara, M., Esposti Ongaro, T., and Neri, A. (2016b). Large eddy simulation of gas–particle kinematic
523 decoupling and turbulent entrainment in volcanic plumes. *Journal of Volcanology and Geothermal
524 Research*
- 525 Compo, G. P., Whitaker, J. S., and Sardeshmukh, P. D. (2006). Feasibility of a 100-year reanalysis using
526 only surface pressure data. *Bulletin of the American Meteorological Society* 87, 175–190
- 527 Compo, G. P., Whitaker, J. S., Sardeshmukh, P. D., Matsui, N., Allan, R. J., Yin, X., et al. (2011). The
528 twentieth century reanalysis project. *Quarterly Journal of the Royal Meteorological Society* 137, 1–28
- 529 Costa, A., Suzuki, Y., Cerminara, M., Devenish, B., Esposti Ongaro, T., Herzog, M., et al. (2016). Results
530 of the eruptive column model inter-comparison study. *Journal of Volcanology and Geothermal Research*
- 531 D'amours, R. (1998). Modeling the etex plume dispersion with the canadian emergency response model.
532 *Atmospheric Environment* 32, 4335–4341
- 533 Daniele, P., Lirer, L., Petrosino, P., Spinelli, N., and Peterson, R. (2009). Applications of the puff model to
534 forecasts of volcanic clouds dispersal from etna and vesuvio. *Computers & Geosciences* 35, 1035–1049
- 535 DeFoor, T. E., Robinson, E., and Ryan, S. (1992). Early lidar observations of the june 1991 pinatubo
536 eruption plume at mauna loa observatory, hawaii. *Geophysical research letters* 19, 187–190
- 537 de'Michieli Vitturi, M., Neri, A., and Barsotti, S. (2015). Plume-mom 1.0: A new integral model of
538 volcanic plumes based on the method of moments. *Geoscientific Model Development* 8, 2447–2463
- 539 Deshler, T., Hofmann, D., Johnson, B., and Rozier, W. (1992). Balloonborne measurements of the pinatubo
540 aerosol size distribution and volatility at laramie, wyoming during the summer of 1991. *Geophysical
541 research letters* 19, 199–202
- 542 Draxler, R. R. and Hess, G. (1998). An overview of the hysplit_4 modelling system for trajectories.
543 *Australian meteorological magazine* 47, 295–308
- 544 Fero, J., Carey, S. N., and Merrill, J. T. (2008). Simulation of the 1980 eruption of mount st. helens using
545 the ash-tracking model puff. *Journal of Volcanology and Geothermal Research* 175, 355–366

- 546 Fero, J., Carey, S. N., and Merrill, J. T. (2009). Simulating the dispersal of tephra from the 1991
547 pinatubo eruption: implications for the formation of widespread ash layers. *Journal of Volcanology and*
548 *Geothermal Research* 186, 120–131
- 549 Folch, A., Costa, A., and Macedonio, G. (2009). Fall3d: A computational model for transport and
550 deposition of volcanic ash. *Computers & Geosciences* 35, 1334–1342
- 551 Folch, A., Costa, A., and Macedonio, G. (2016). Fplume-1.0: An integral volcanic plume model accounting
552 for ash aggregation. *Geoscientific Model Development* 9, 431
- 553 Guo, S., Bluth, G. J., Rose, W. I., Watson, I. M., and Prata, A. (2004a). Re-evaluation of so₂ release
554 of the 15 june 1991 pinatubo eruption using ultraviolet and infrared satellite sensors. *Geochemistry,*
555 *Geophysics, Geosystems* 5
- 556 Guo, S., Rose, W. I., Bluth, G. J., and Watson, I. M. (2004b). Particles in the great pinatubo volcanic cloud
557 of june 1991: The role of ice. *Geochemistry, Geophysics, Geosystems* 5
- 558 Holasek, R., Self, S., and Woods, A. (1996a). Satellite observations and interpretation of the 1991 mount
559 pinatubo eruption plumes. *Journal of Geophysical Research: Solid Earth* 101, 27635–27655
- 560 Holasek, R. E., Woods, A. W., and Self, S. (1996b). Experiments on gas-ash separation processes in
561 volcanic umbrella plumes. *Journal of volcanology and geothermal research* 70, 169–181
- 562 Jäger, H. (1992). The pinatubo eruption cloud observed by lidar at garmisch-partenkirchen. *Geophysical*
563 *research letters* 19, 191–194
- 564 Mastin, L. G. (2007). A user-friendly one-dimensional model for wet volcanic plumes. *Geochemistry,*
565 *Geophysics, Geosystems* 8
- 566 Neri, A., Esposti Ongaro, T., Macedonio, G., and Gidaspow, D. (2003). Multiparticle simulation of
567 collapsing volcanic columns and pyroclastic flow. *Journal of Geophysical Research: Solid Earth*
568 (1978–2012) 108
- 569 Oberhuber, J. M., Herzog, M., Graf, H.-F., and Schwanke, K. (1998). Volcanic plume simulation on large
570 scales. *Journal of Volcanology and Geothermal Research* 87, 29–53
- 571 Paladio-Melosantos, M. L. O., Solidum, R. U., Scott, W. E., Quiambao, R. B., Umbal, J. V., Rodolfo, K. S.,
572 et al. (1996). Tephra falls of the 1991 eruptions of mount pinatubo. *Fire and mud* 12000, 12030
- 573 Pouget, S., Bursik, M., Singla, P., and Singh, T. (2016). Sensitivity analysis of a one-dimensional model of
574 a volcanic plume with particle fallout and collapse behavior. *Journal of Volcanology and Geothermal*
575 *Research*
- 576 Rolph, G., Stein, A., and Stunder, B. (2017). Real-time environmental applications and display system:
577 Ready. *Environmental Modelling & Software* 95, 210–228
- 578 Schwaiger, H. F., Denlinger, R. P., and Mastin, L. G. (2012). Ash3d: A finite-volume, conservative
579 numerical model for ash transport and tephra deposition. *Journal of Geophysical Research: Solid Earth*
580 117
- 581 Scott, W. E., Hoblitt, R. P., Torres, R. C., Self, S., Martinez, M. M. L., and Nillos, T. (1996). Pyroclastic
582 flows of the june 15, 1991, climactic eruption of mount pinatubo. *Fire and Mud: eruptions and lahars of*
583 *Mount Pinatubo, Philippines*, 545–570
- 584 Searcy, C., Dean, K., and Stringer, W. (1998). Puff: A volcanic ash tracking and prediction model. *Journal*
585 *of Volcanology and Geothermal Research* 80, 1–16
- 586 Self, S., Zhao, J.-X., Holasek, R. E., Torres, R. C., and King, A. J. (1996). The atmospheric impact of the
587 1991 mount pinatubo eruption
- 588 Stein, A., Draxler, R., Rolph, G., Stunder, B., Cohen, M., and Ngan, F. (2015). Noaa's hysplit atmospheric
589 transport and dispersion modeling system. *Bulletin of the American Meteorological Society* 96, 2059–
590 2077

Table 1. Three different methods for creating initial conditions (initial ash clouds) for Puff simulation

	No model	1D model	3D model
Maximum height	Calibration	Semiempirical	1st principle
Average height	Calibration	Conservation (1D)	laws 1st principle
Vertical spread	Calibration	Semiempirical	1st principle
Column radius	Calibration	Conservation (1D)	laws 1st principle
Plume shape	Semiempirical	Semiempirical	1st principle
Tracers number	Free parameter	Free Parameter	Based on simulation

- 591 Stohl, A., Prata, A., Eckhardt, S., Clarisse, L., Durant, A., Henne, S., et al. (2011). Determination of
 592 time-and height-resolved volcanic ash emissions and their use for quantitative ash dispersion modeling:
 593 the 2010 eyjafjallajökull eruption. *Atmospheric Chemistry and Physics* 11, 4333–4351
- 594 Suzuki, T. et al. (1983). A theoretical model for dispersion of tephra. *Arc volcanism: physics and tectonics*
 595 95, 113
- 596 Suzuki, Y. and Koyaguchi, T. (2009). A three-dimensional numerical simulation of spreading umbrella
 597 clouds. *Journal of Geophysical Research: Solid Earth (1978–2012)* 114
- 598 Suzuki, Y. J., Koyaguchi, T., Ogawa, M., and Hachisu, I. (2005). A numerical study of turbulent mixing
 599 in eruption clouds using a three-dimensional fluid dynamics model. *Journal of Geophysical Research: Solid Earth* 110
- 600 Tanaka, H. (1991). Development of a prediction scheme for the volcanic ash fall from redoubt volcano. In
 601 *First Int'l. Symp. on Volcanic Ash and Aviation Safety*. vol. 58
- 602 Tupper, A., Itikarai, I., Richards, M., Prata, F., Carn, S., and Rosenfeld, D. (2007). Facing the challenges of
 603 the international airways volcano watch: the 2004/05 eruptions of manam, papua new guinea. *Weather and Forecasting* 22, 175–191
- 604 Walko, R., Tremback, C., and Bell, M. (1995). Hypact: The hybrid particle and concentration transport
 605 model. *User's guide*
- 606 Whitaker, J. S., Compo, G. P., Wei, X., and Hamill, T. M. (2004). Reanalysis without radiosondes using
 607 ensemble data assimilation. *Monthly Weather Review* 132, 1190–1200
- 608 Witham, C., Hort, M., Potts, R., Servranckx, R., Husson, P., and Bonnardot, F. (2007). Comparison of
 609 vaac atmospheric dispersion models using the 1 november 2004 grimsvötn eruption. *Meteorological Applications* 14, 27–38
- 610 Woods, A. (1988). The fluid dynamics and thermodynamics of eruption columns. *Bulletin of Volcanology*
 611 50, 169–193
- 612 Zidikheri, M. J., Lucas, C., and Potts, R. J. (2017). Estimation of optimal dispersion model source
 613 parameters using satellite detections of volcanic ash. *Journal of Geophysical Research: Atmospheres*
 614 122, 8207–8232

FIGURE CAPTIONS

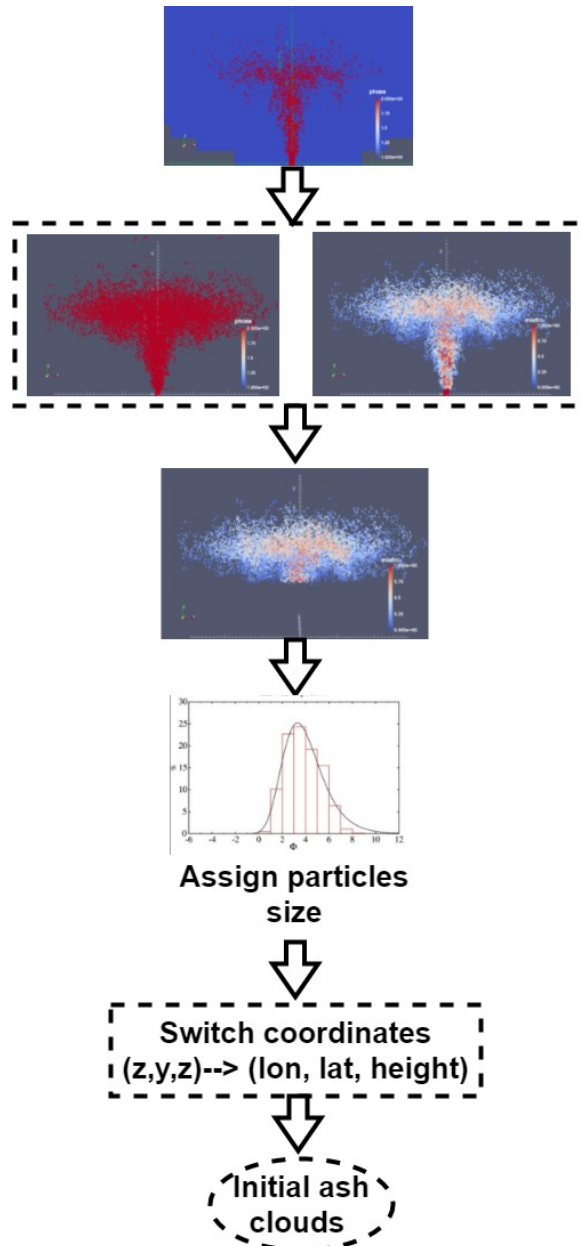


Figure 1. Steps to create initial condition for Puff based on raw output of Plume-SPH (Cao et al., 2018). First row: raw output of Plume-SPH. Blue particles are phase 1 (ambient air), red particles are phase 2 (erupted material). Second row: plume after removing SPH particles of phase 1. Picture at right is colored according to the mass fraction of erupted material. Third row: volcanic plume above the ‘‘corner’’ region after cutting off the lower portion. Fourth row: assign sizes to particles converting numerical discretization points into tracers. Fifth row: switch coordinates in local coordinate system into (*longitude, latitude, height*)

Table 2. The starting and ending time (UT) for simulating the climactic phase of Pinatubo eruption on June 15 1991. Observed plume height (Holasek et al., 1996a) at different time are also listed in the table.

Eruption duration	4.9 hours	9 hours	10 hours	11.1 hours
Start time	0441	0441	0441	0334
Height at start time	37.5 km	37.5 km	37.5 km	24.5 km
End time	0934	1341	1441	1441
Height at end time	35 km	26.5 km	22.5	22.5 km

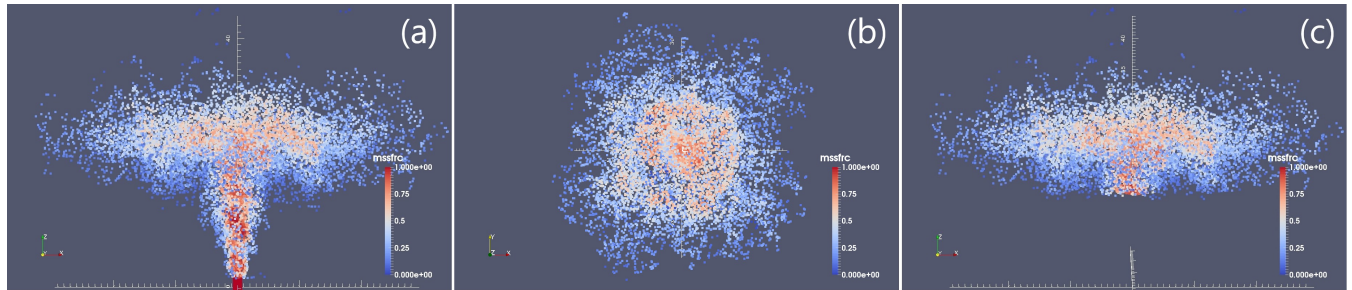


Figure 2. Volcano plume from 3D plume model. All particles in the pictures are of phase 2 (particle of phase 1 has been removed) at 600s after eruption, at which time, the plume has already reached the maximum height and started spreading radially. (a) is front view of the whole plume. (b) top view of the plume. (c) is front view of the initial ash cloud, which is essentially a portion of the whole plume with elevation higher than a given threshold (in this picture is 15000m). Particles are colored according to mass fraction of erupted material. Red represents high mass fraction while blue represents low mass fraction.

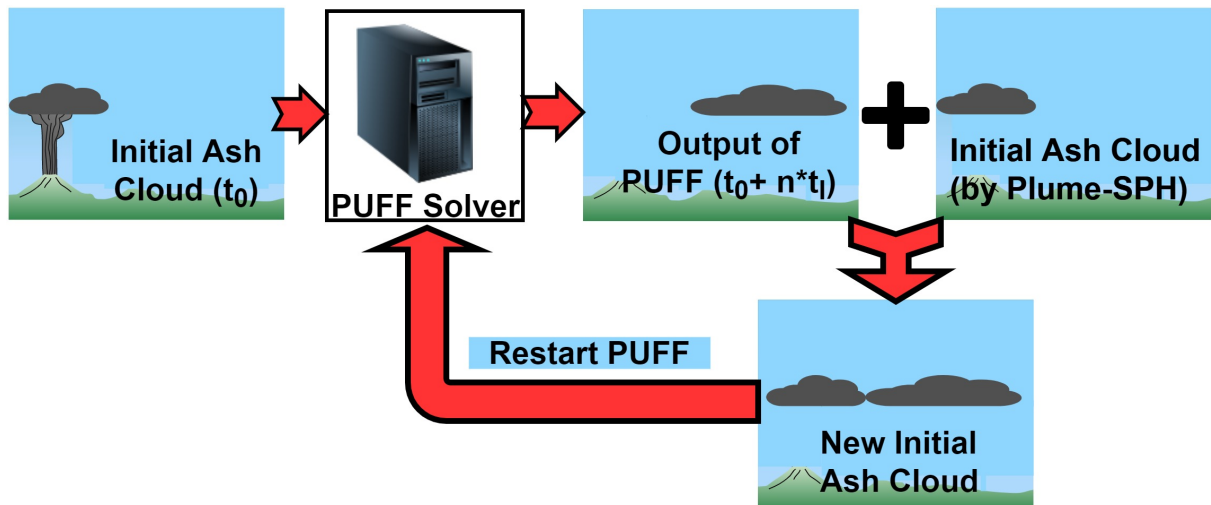


Figure 3. Mimic successive eruption with intermittent pulsed releasing of ash particles. t_l is the period of pulsing release. t_l equals the physical time of 3D plume simulation.

Table 3. List of eruption condition and material properties for plume simulation

Parameters	Units	Plume
Vent velocity	$m \cdot s^{-1}$	275
Vent gas mass fraction		0.05
Vent Temperature	K	1053
Vent height	m	1500
Mass discharge rate	$kg \cdot s^{-1}$	1.5×10^9
Specific heat of gas at constant volume	$J \cdot kg^{-1} \cdot K^{-1}$	717
Specific heat of air at constant volume	$J \cdot kg^{-1} \cdot K^{-1}$	1340
Specific heat of solid	$J \cdot kg^{-1} \cdot K^{-1}$	1100
Specific heat of gas at constant pressure	$J \cdot kg^{-1} \cdot K^{-1}$	1000
Specific heat of air at constant pressure	$J \cdot kg^{-1} \cdot K^{-1}$	1810
Density of air at vent height	$kg \cdot m^{-3}$	1.104
Pressure at vent height	Pa	84363.4

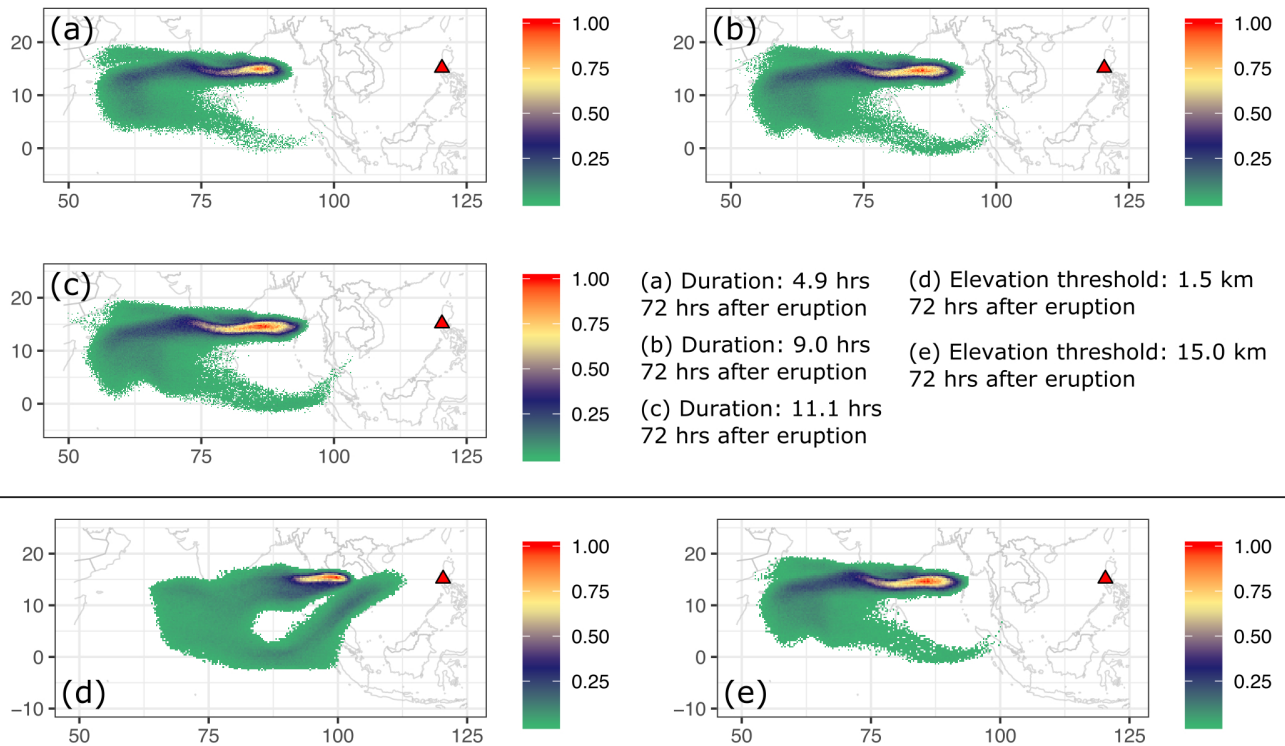


Figure 4. Sensitivity of Puff simulation with respect to eruption durations and initial ash cloud cutoff heights .(a) to (c) are simulated ash distribution with different starting and ending time. They corresponding to eruption duration of 4.9 hours, 9 hours and 11.1 hours respectively. Starting and ending time for each case is in Table 2. (d) and (e) are simulated ash distribution taking initial ash clouds obtained using different elevation thresholds (1500m and 15000 m) from output of Plume-SPH. The starting and ending time are corresponding to 9 hours duration case in Table 2. The contours correspond to ash concentration at 72 hours after eruption.

Table 4. Parameters used in VATD simulation of the climactic phase of Pinatubo eruption on June 15 1991. The first six parameters are used by semiempirical expression to create an initial ash cloud. When creating an initial condition based on the Plume-SPH model, these parameters are extracted from output of Plume-SPH model.

Parameters	Unit	Semiempirical	Plume-SPH
Maximum Height (H_{max})	m	40000	41800
Horizontal Spread (r_{max})	km	103.808	-
Vertical Spread (H_{width})	km	6.662	-
Plume Shape	-	Poisson	-
Total Ash Particles	-	1768500	1768500
Elevation Threshold	m	-	15000
Horizontal Diffusivity	m^2/s	10000	10000
Vertical Diffusivity	m^2/s	10	10
Grain Size Distribution	-	Gaussian	Gaussian
Mean of Grain Size (Radius)	mm	3.5×10^{-2}	3.5×10^{-2}
Standard Deviation of Grain Size	-	1.0	1.0
Start Time	UT	0441	0441
End time	UT	1341	1341
Simulation Duration	hour	72	72

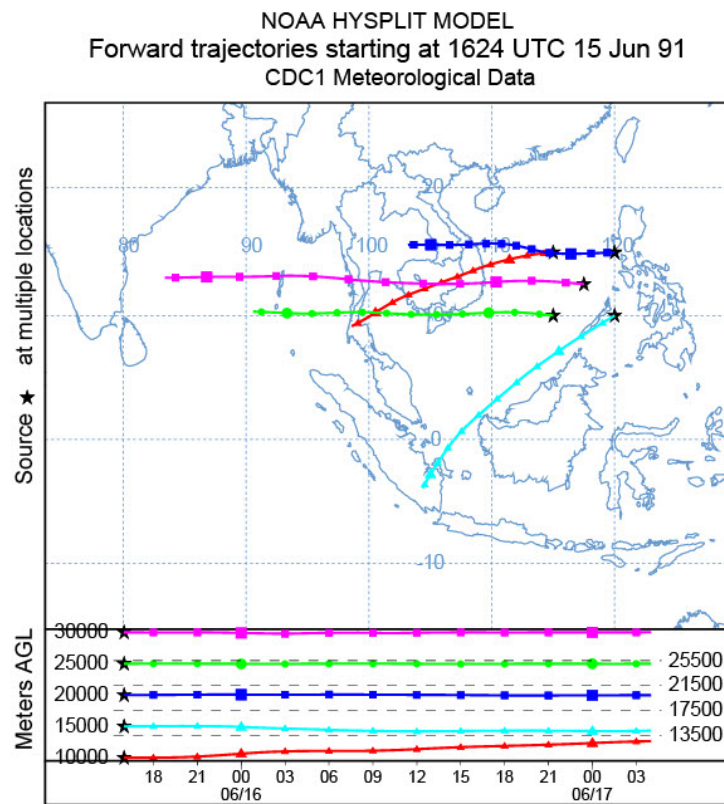


Figure 5. Trajectories of particles starting from different heights indicating the wind directions of different evaluations.

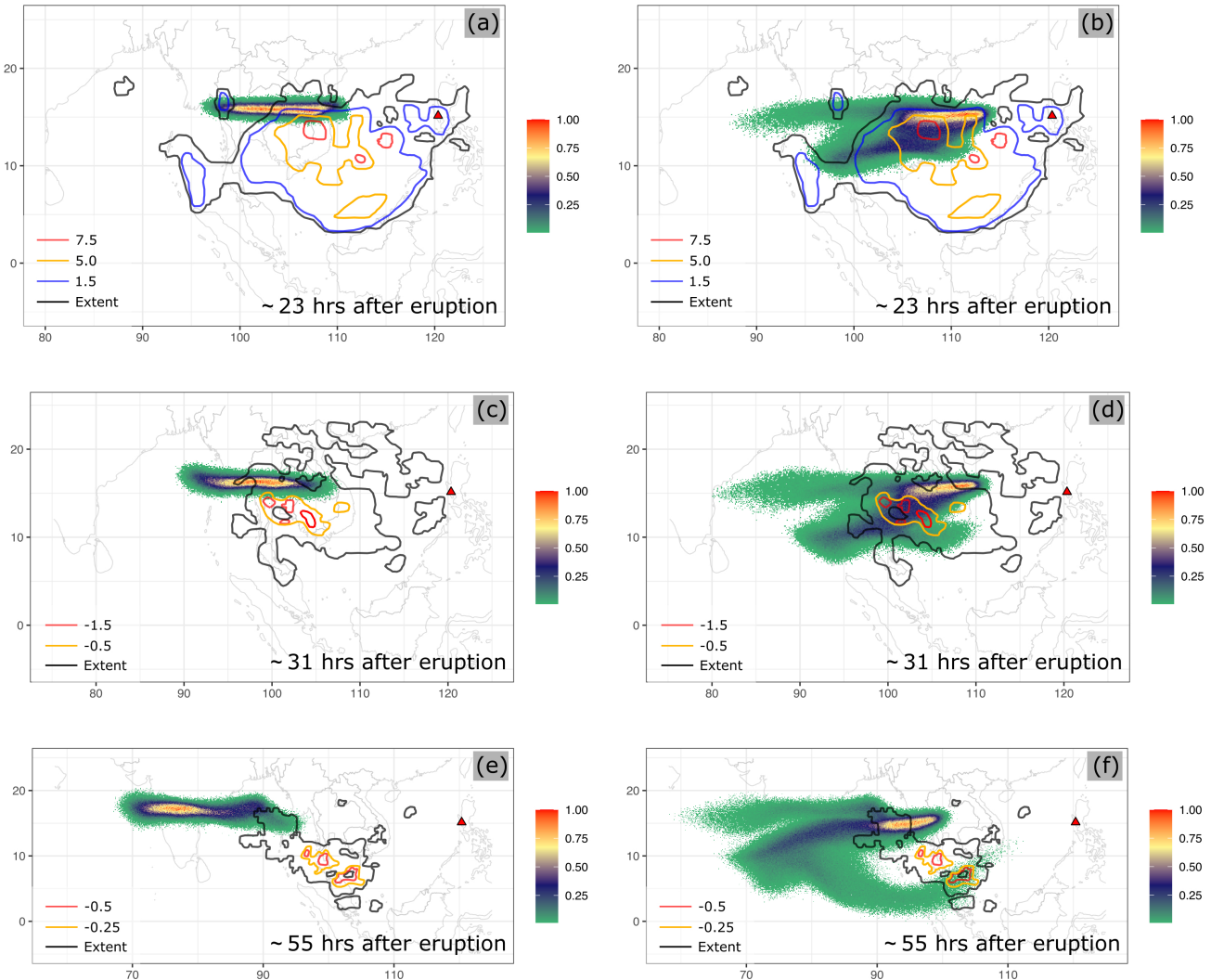


Figure 6. Comparison between “Semiempirical initial cloud + Puff” and “Plume-SPH + Puff”. Pictures to the left are: Puff simulation based on initial condition created according to semiempirical plume shape expression. Pictures to the right are Puff simulation based on initial condition generated by Plume-SPH. TOMS or AVHRR image of Pinatubo ash cloud are overlapped with the simulation results. Ash clouds at different hours after eruption are on different rows. From top to bottom, the images are corresponding to around 23 hours after eruption (UT 199106160341), 31 hours after eruption (UT 199106161141), 55 hours after eruption (UT 199106171141). The observation data on the first row are TOMS ash and ice map. The observation data on the second and third row are AVHRR BTD ash cloud map with atmospheric correction method applied (Guo et al., 2004b).

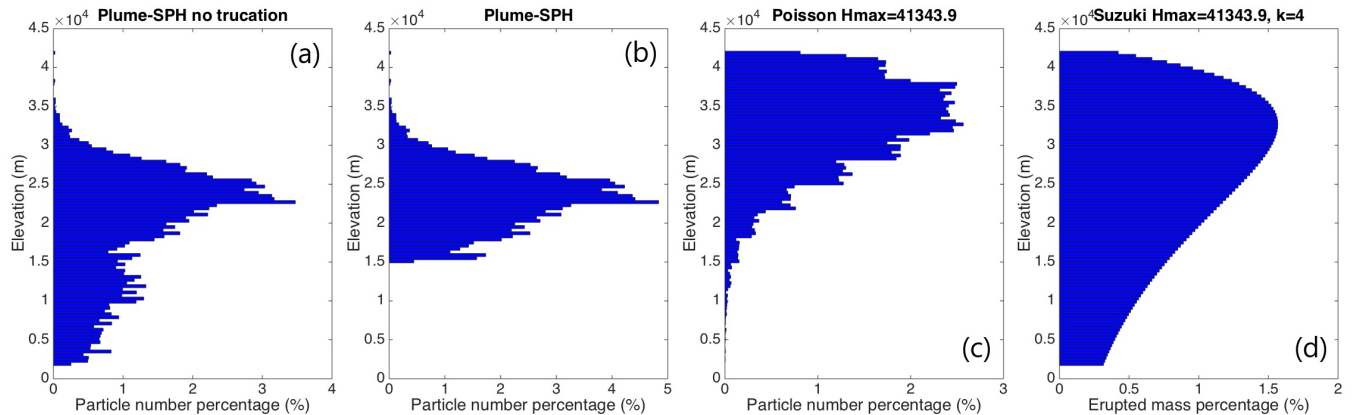


Figure 7. Particle distribution of initial ash cloud in vertical direction. (a) is corresponding to the initial ash cloud obtained from Plume-SPH output. (b) is corresponding to ash distribution of Plume-SPH output truncated by a elevation threshold of 15000m. (c) is for vertical ash distribution based on Poisson distribution with maximum height equals to 40000m. Another parameter, the vertical spread, in the expression of Poisson plume shape is 6662m. (d) is corresponding to Suzuki distribution with maximum height equals to 40000m. Another parameter in Suzuki distribution, the shape factor, is 4. The x axis is the percentage of particle numbers for Plume-SPH and Poisson. For Suzuki the x axis is the mass percentage of erupted material.

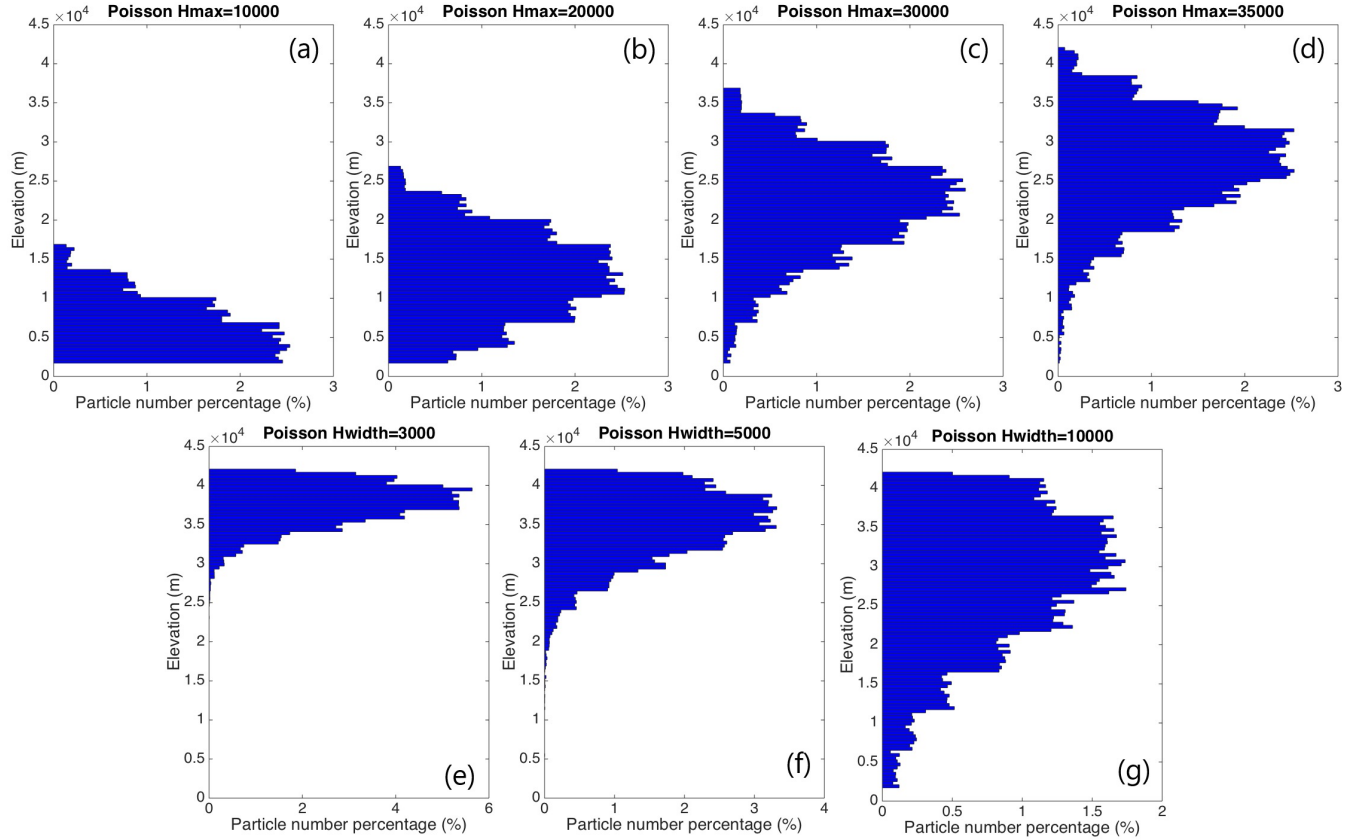


Figure 8. Initial particle distribution in vertical direction based on Poisson plume shape. The first row varies maximum heights. (a) to (d) are corresponding to maximum height of 10000m, 20000m, 30000m, 35000m. Another parameter, the vertical spread, in the expression of Poisson plume shape is 6662m for all four figures in the first row. The second row varies “vertical spread”. (e) to (g) are corresponding to vertical spread of 3km, 5km and 10km. The maximum height in the expression of Poisson plume shape is 40000m for all three figures. The x axis is the percentage of particle numbers. See Fig. 7 for vertical ash distribution of Plume-SPH output.

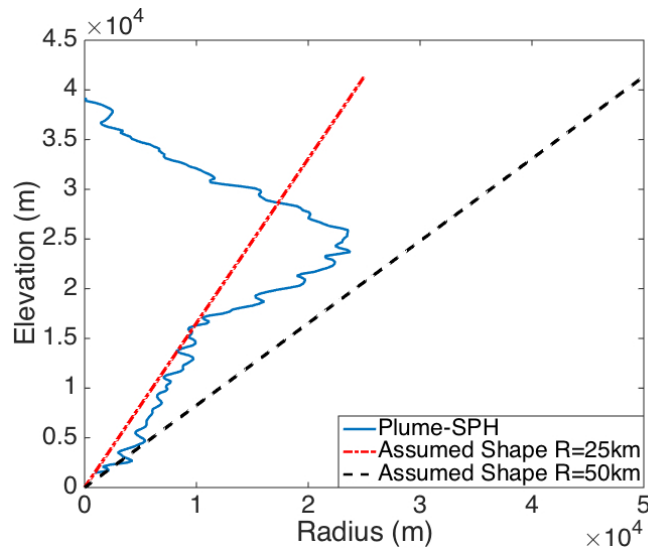


Figure 9. Comparison between radius of initial ash clouds created by 3D plume model (Plume-SPH) and assumed initial ash cloud shape in Puff. The plume shape expression used in Puff defines an inverted cone whose actual shape changes when “horizontal spread” takes different values. $R = 25\text{km}$ is corresponding to “horizontal spread” equals to 50km . $R = 50\text{km}$ is corresponding to “horizontal spread” equals to 100km

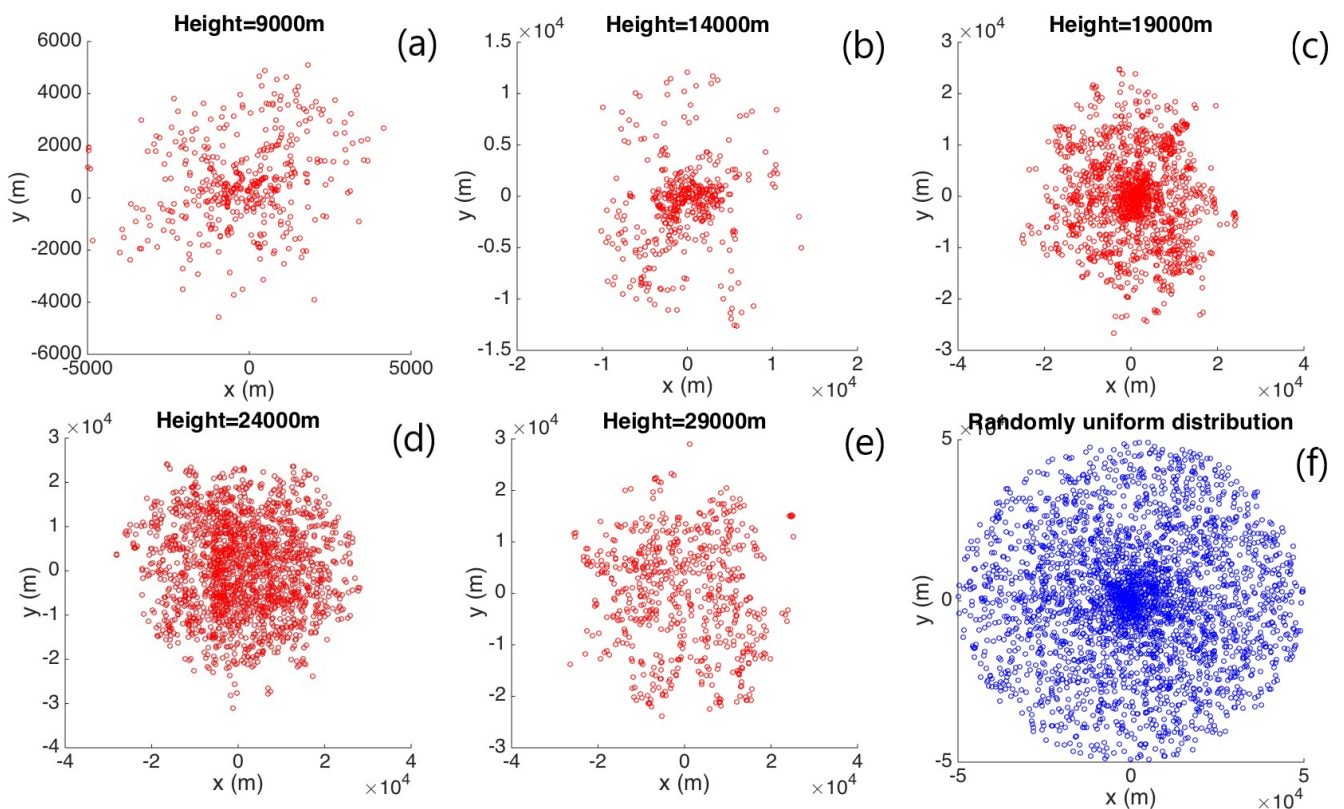


Figure 10. Horizontal distribution of ash particles (tracers) on a cross section of initial ash cloud. Puff assumes a randomly uniform distribution of ash particles within a circle, as shown by blue dots in (f). All other figures show the ash particle distribution of initial ash clouds created by Plume-SPH at different elevations.

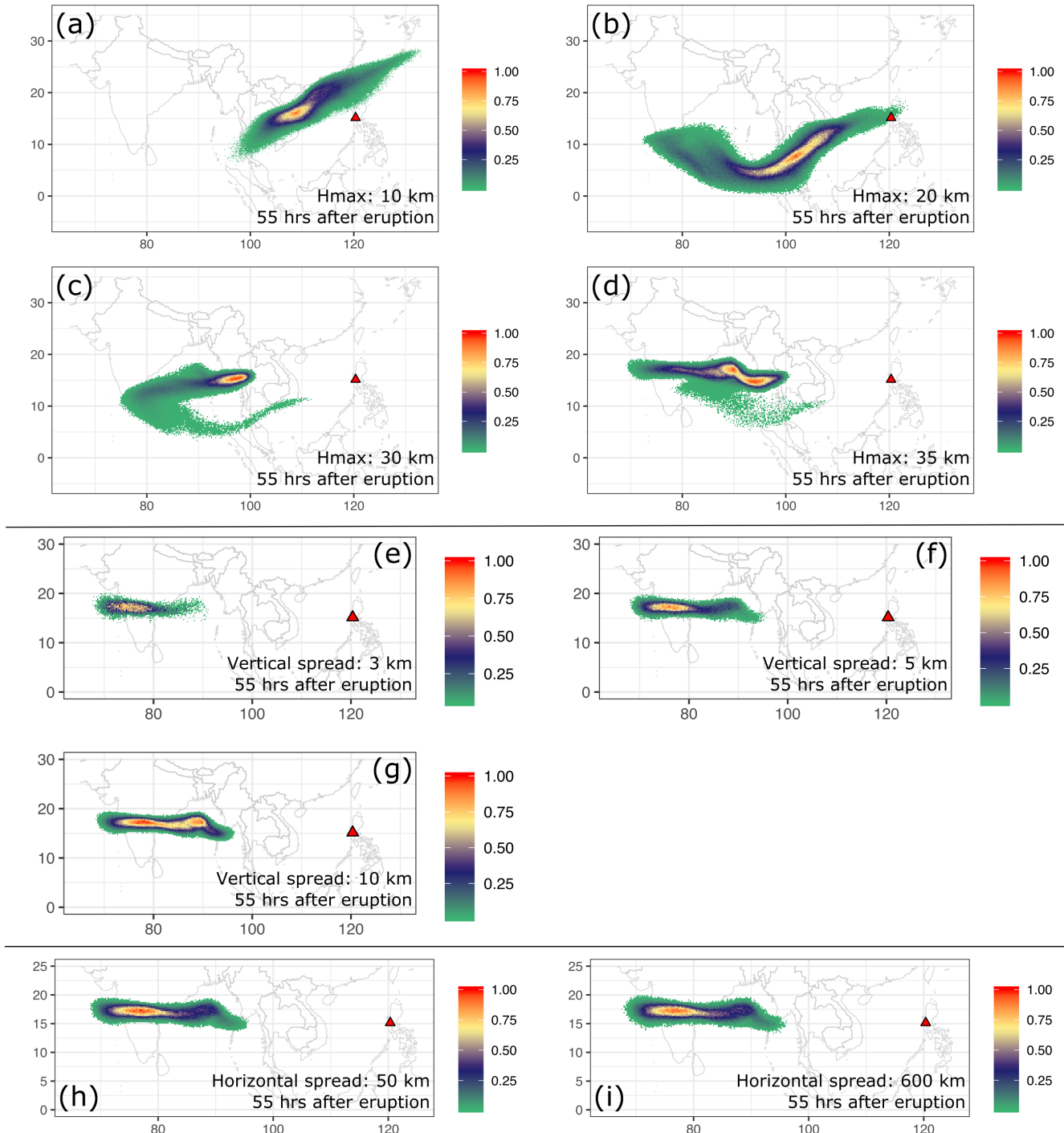


Figure 11. Ash transport simulated by Puff using different initial ash clouds created according the empirical expressions. Initial ash cloud for (a) to (d) are created according to Poisson distribution with maximum plume heights of 10km, 20km, 30km and 35km respectively. Initial ash cloud for (e) to (g) are created with vertical spread equals to 3km, 5km and 10km. respectively. Initial ash cloud for (h) - (i) are created with “horizontal spread” equals to 50km and 600km respectively. All images are for simulated ash transport around 55 hours after eruption (UT 199106171141). See the observed cloud image in Fig. 6.